Development of Advanced Computational Aeroelasticity Tools at NASA Langley Research Center

R. E. Bartels
NASA Langley Research Center
Hampton, VA 23681

Robert.E.Bartels@nasa.gov

ABSTRACT

NASA Langley Research Center has continued to develop its long standing computational tools to address new challenges in aircraft and launch vehicle design. This paper discusses the application and development of those computational aeroelastic tools. Four topic areas will be discussed: 1) Modeling structural and flow field nonlinearities; 2) Integrated and modular approaches to nonlinear multidisciplinary analysis; 3) Simulating flight dynamics of flexible vehicles; and 4) Applications that support both aeronautics and space exploration.

1.0 INTRODUCTION

New innovative aerospace vehicle designs, such as are required for long endurance and highly maneuverable aircraft or for inflatable decelerators for atmospheric reentry, have necessitated advances in the methods of computational aeroelasticity. The analysis of structural nonlinearity such as that caused by control surface free play has also motivated methodological advances. The initiation of the design of a new launch vehicle for human space exploration also provides a challenge to existing computational aeroelastic tools. Launch vehicle design that includes bluff body protuberances and in a flight path including large angle of attack variations leads to the possibility of unsteady transonic and separated flows that can interact with a slender, highly flexible structure. NASA Langley Research Center has continued to develop its long standing computational tools to address new challenges in aircraft and launch vehicle design.

There are several NASA computational fluid dynamics (CFD) codes that have the capability to simulate aeroelastic phenomena. The transonic small disturbance codes CAP-TSD[1] and CAP-TSDv[2,3] are widely used as rapid methods for simulating dynamic aeroelasticity for relatively simple configurations. The structured Euler/Navier-Stokes code CFL3D v6.4[4] has been widely used in recent years as a means of aeroelastic simulation for vehicles having a more complex geometry. Recently the unstructured NASA code FUN3D[5,6] has been given aeroelastic capability as well.

This paper will focus on the use of CFL3D and FUN3D as tools for aeroelastic analysis. Four areas of recent development will be discussed in this paper: 1) Modeling structural and flow field nonlinearities; 2) Integrated and modular approaches to nonlinear multidisciplinary analysis; 3) Simulating flight dynamics of flexible vehicles; and 4) Applications that support both aeronautics and space exploration.

2.0 MODELING STRUCTURAL AND FLOW FIELD NONLINEARITIES

The accurate prediction of limit cycle oscillation (LCO), transonic flutter, buffet, and buzz remains a challenge. It is generally accepted that these nonlinear phenomena are caused by a linear instability combined with nonlinearities in the fluid, the structure, or both. LCO, for example, is thought to be caused by nonlinear flow due to large shock motion or flow separation, or structural nonlinearities arising from freeplay in hinges and linkages of control surfaces or from material behavior. Aging aircraft and combat aircraft carrying heavy external stores are known to experience LCO, typically due to structural nonlinearities. In the past two decades considerable efforts have been devoted to the development of aeroelastic tools that model flow field nonlinearity. The capability to couple flow field and structural nonlinearities and the accurate prediction of nonlinearity induced phenomena is however in its infancy. Recent work has focused on the modeling of LCO induced by structural freeplay. In our work, structural freeplay has been modeled using a nonlinear Navier-Stokes flow field solver[4] and a modal representation of the equations of structural dynamics that include freeplay. The model and experimental data are taken from ref.s 7-8. Reference 9 presents the present analysis in more detail.

The aeroelastic equations of motion for a structural model of control surface freeplay can be written as,

$$\mathbf{m}\ddot{\boldsymbol{\delta}} + \mathbf{d}\dot{\boldsymbol{\delta}} + \mathbf{k}\boldsymbol{\delta} + \mathbf{k}\hat{\boldsymbol{\delta}} = \mathbf{f} \tag{1}$$

where $\mathbf{m}$, $\mathbf{d}$, and $\mathbf{k}$ are the mass, damping, and stiffness matrices; $\boldsymbol{\delta}$ is the physical displacements vector and $\mathbf{f}$ is the aerodynamic forces vector. For modes i with freeplay

$$\hat{\delta}_i = \begin{cases} -\delta_{0i} & , \quad \delta_i > +\delta_{0i} \\ -\delta_i & , \quad |\delta_i| \le +\delta_{0i} \\ +\delta_{0i} & , \quad \delta_i < -\delta_{0i} \end{cases} \tag{2}$$

and, for modes j without freeplay $\hat{\delta}_j = 0$. Note that equations 1 and 2 can be easily modified to model asymmetric freeplay behavior. In equation (1), the restoring torque due to freeplay is modeled as the sum of a linear term $(\mathbf{k}\boldsymbol{\delta})$ and a nonlinear residual term $(\mathbf{k}\hat{\boldsymbol{\delta}})$.

There is a clear advantage in modeling control surface freeplay using the normal modes of the structure. Computing the effect of freeplay as a modal residual allows application of this technique to complex aircraft for which only normal modes of the structural model are available. It also offers a significant reduction in the computing required as compared to computing with a full finite element or stiffness model. Accordingly, after moving the residual term to the right hand side and performing a modal transformation based on the equations without freeplay, equation (1) is generalized to

$$\mathbf{M}\ddot{\mathbf{q}} + \mathbf{D}\dot{\mathbf{q}} + \mathbf{K}\mathbf{q} = \mathbf{F} - \boldsymbol{\phi}^{\mathrm{T}}\mathbf{k}\hat{\boldsymbol{\delta}} \tag{3}$$

where $\boldsymbol{\phi}$ are the eigenvectors of the system $\mathbf{m}\ddot{\boldsymbol{\delta}} + \mathbf{k}\boldsymbol{\delta} = \mathbf{0}$. **M**, **D**, **K** and **F** are the generalized mass, damping, stiffness and force. $\boldsymbol{\phi}^{\mathrm{T}}\mathbf{k}\hat{\boldsymbol{\delta}}$ is the generalized residual force. In the absence of freeplay, this term would be zero.

Simulations have been performed with CFL3D for a NACA 0012 airfoil with pitch/plunge degrees of freedom and a trailing edge control surface having torsional stiffness with freeplay. Comparisons of Navier-Stokes simulations with experimental results (from ref. 8) and numerical results using a linear unsteady aerodynamic model (ref. 7) are shown in Figure 1. The upper half of the figure shows the CFL3D Navier-Stokes results from ref. 9 while the lower half of the figure shows experimental and the linear aerodynamics simulation results. Of the results in the lower half of the figure, the dark lines are experimental data while the light lines are numerical results. The Mach number was in the range of $0.02 < M_\infty < 0.07$ and the velocity varied between 7 and 23 meters per second. The Reynolds number based on chord was in the range of 500,000. Note that at this Reynolds number much of the airfoil is likely to be laminar or transitional, although the present computations were fully turbulent. The scale, U/U_f referred to as the speed-ratio, is the ratio of the flow speed to the linear flutter speed. Five types of system behavior were observed experimentally and computationally. The speed ranges of these five types of behavior are indicated by the upper and lower color bars in Figure 1. The upper color bars indicate the system behavior simulated by CFL3D while the lower color bars indicate system behaviors in the experiment. There are discrepancies in the onset speeds for the various behaviors, however, overall the stages described by the experiment are also seen in the CFD simulation.

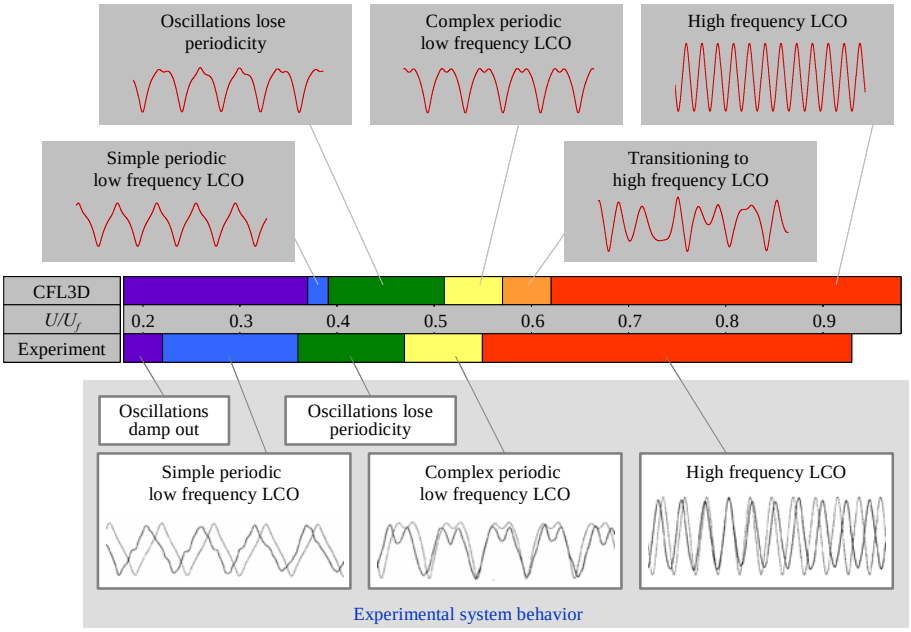

Figure 1. Limit cycle oscillations of pitch plunge airfoil with control surface free-play. (From ref. 9)

3.0 INTEGRATED AND MODULAR APPROACHES TO NONLINEAR MULTIDISCIPLINARY ANALYSIS

Traditionally computational aeroelasticity codes have integrated the flow field and structure solvers in a single monolithic code. This integration has performed well for applications that are amenable, for instance, to a modal structural decomposition. Such a modal representation of the structure can be easily integrated into a CFD code. The treatment of mesh deformations using a shearing, a transfinite-interpolation or a simple spring or elasticity-based scheme works well for small to moderate smoothly varying deflections. These mesh deformation schemes have typically been integrated into a CFD code. However, as the complexity of

problems has grown, the complexity of the analysis packages required for the structural modeling, flow field modeling and mesh motion has grown. Likewise the computing power available to address these more complex problems has grown.

These growth factors have resulted in the emergence of methods of coupling software packages in loosely coupled or quasi-close coupled multidisciplinary analyses. Figure 2 illustrates an approach to mesh adaptation, repair and regeneration that has recently been successfully applied by the author using CFL3D to simulate the flight of a moderately flexible vehicle with a range of complex surface motions. To move the CFD mesh in response to vehicle motion and deformation, CFL3D first moves grid control points and then performs transfinite interpolation of the remaining mesh points. As needed the commercial software package Gridgen™ (manufactured by Pointwise™ Inc.) is called within CFL3D to repair small regions of the grid that are not successfully moved by the internal mesh scheme. This approach combines the speed of an algebraic mesh motion scheme to perform the majority of the mesh movement with the intermittent use of the grid repair capability of a commercial software package. This approach has been used to simulate the static and dynamic aeroelastic response of an innovative supersonic transport conceptual design under development by the Lockheed Martin Company. The body freedom flutter analysis of this configuration has been performed to compute flutter onset through the transonic regime where traditional linear flutter onset tools are generally inadequate. Figure 3 shows the MSC.Nastran™ finite element model used in this work. MSC.Nastran™ is manufactured by the MSC.Software Corporation. Figure 4 presents the static aeroelastic deflected shape of the supersonic transport at Mach 0.98 and 1g trim. The large deflections of the inboard trailing edge flap induced by the flow through the inverted V-tail/inboard wing area illustrate the challenges presented by this aircraft design.

The unstructured code FUN3D uses an elasticity based scheme to deform the mesh that is internal to the code but also has the capability to perform mesh regeneration using an external commercial grid tool. There are several approaches available in FUN3D for adaptation of a grid to improve the accuracy and quality of a CFD solution. Reference 10 discusses solution gradient-based grid adaptation tools for use with the FUN3D code. References 11 and 12 discuss adjoint-based error estimation and grid adaptation in FUN3D. An in-code approach to grid adaptation is available in FUN3D that uses a simple spring-analogy mesh movement algorithm that moves mesh points toward regions of flow gradient such as a shock. This method and another approach which adds and/or removes cells based on flow field gradients, both of which are available with FUN3D, were used by reference 10 to compute the supersonic and hypersonic flow field around an atmospheric entry vehicle. To allow better grid resolution at a surface, the latter mesh adaptation scheme interfaces with a high fidelity surface CAD representation using GridEx[13] (developed by the NASA Langley Research Center Geometry Laboratory) and the coupling software Computational Analysis PRogramming Interface (CAPrI).[14] This version of CAPrI is bundled with GridEx and was originally developed by the Massechusetts Institute of Technology.

New challenges to the aeroelastician are presented by the recent interest in inflatable thin membrane atmospheric entry decelerators. One such decelerator is the clamped ballute. One of the challenges is the modeling of the ballute's complex hypersonic flow field. Because of the size and flexibility of the clamped ballute membrane, an aeroelastic analysis must take into account unsteady hypersonic shock/membrane interactions. The large deflections of the 3-dimensional membrane structure that include membrane wrinkling and thermal creep present challenges to a structural solver. In the most general sense a dynamic structural model that includes geometric and material nonlinearity and aerothermoelastic interactions is required. Recent efforts at modeling both the static and dynamic aeroelastic behavior of a ballute are found in References 15-17. In those references, static aeroelastic modeling is performed by iteratively coupling a Cartesian Euler code with a nonlinear structural solver. Dynamic aeroelastic modeling is performed by a

quasi-steady analysis of the motion of the fluid/structure interaction. The present author's group has proposed modeling the geometric and material nonlinearity and thermoelastic behavior of the membrane statically while modeling the flutter onset by a normal modes analysis about the nonlinear static solution. [18]

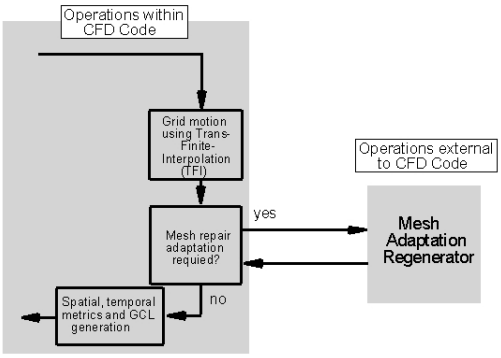

Figure 2. Schematic of mesh deformation/adaption and grid repair.

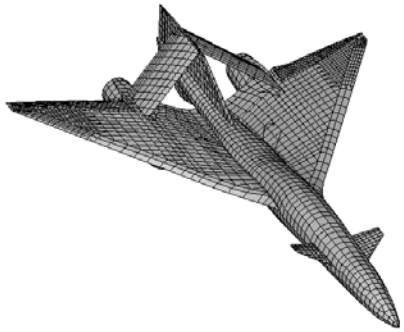

Figure 3. Supersonic transport MSC.Nastran™ finite element model.

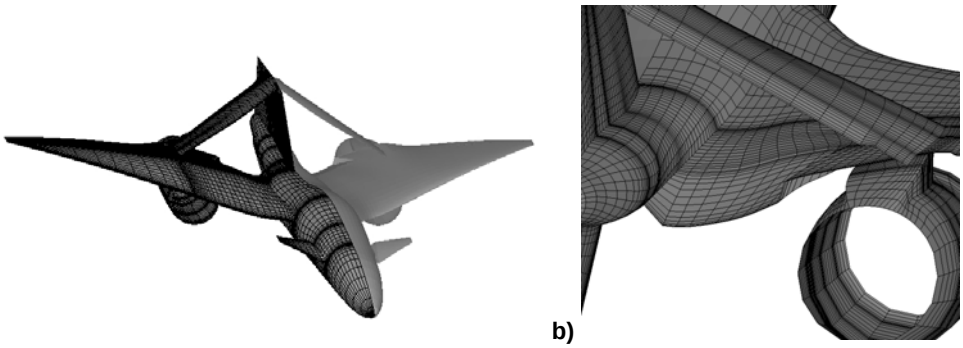

a) **b)**

Figure 4. Supersonic transport CFD surface mesh for flexible vehicle at Mach 0.98, 1g trimmed. a) Full vehicle surface, b) Inboard flap detail.

Figure 5 shows the coupling of a nonlinear flow field code and a commercially available linear or nonlinear structural solver. This is the approach used by our group in the static aerothermoelastic modeling of a nonlinear membrane structure.[19] As initial steps toward the capability to model a full 3-dimensional membrane structure, Figure 6 shows the static aeroelastic solution of a 2D membrane with pretension and an upper/lower side pressure difference subject to a Mach 5.0 flow field. The normal modes analysis performed in reference 19 and shown in Figure 7 indicates that mode shapes and frequencies significantly differ at different altitudes due to the variation of static membrane shapes with dynamic pressure. Due to the nonlinear

variation of the ballute shape with altitude loose coupling of at least the static aerothermoelastic behavior if not the full dynamic behavior of the ballute, using a nonlinear CFD code and a nonlinear structural code is required.

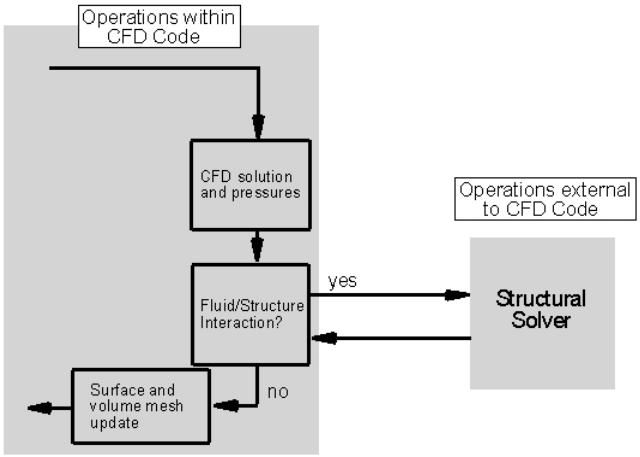

Figure 5. Schematic of fluid/structure interaction using an external structural solver.

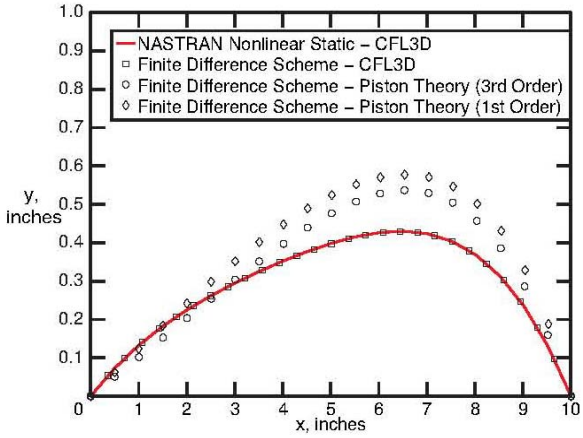

Figure 6. Static deflection of a membrane due to a Mach 5.0 flow field. (From Ref. 19)

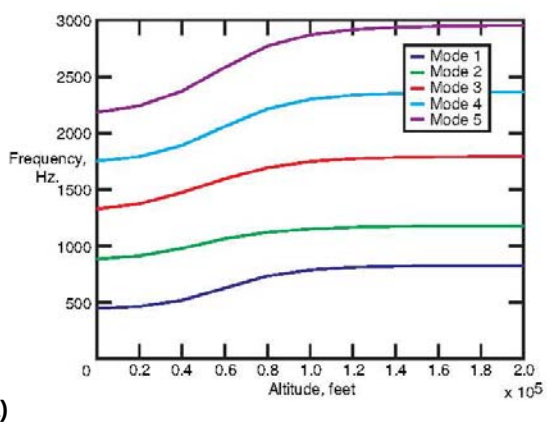

a)

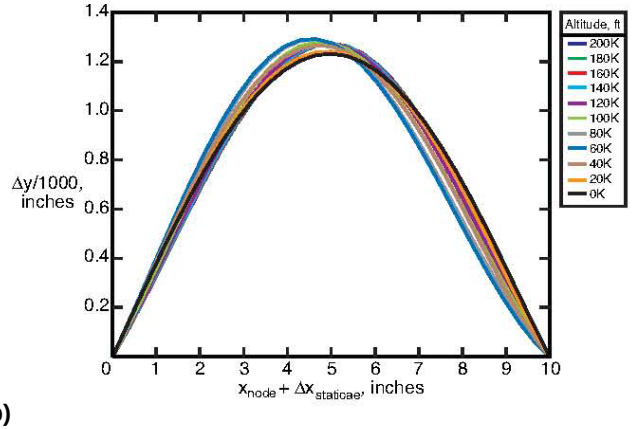

b)

**Figure 7. Normal modes analysis for membrane in a Mach 5.0 flow field.
(From Ref. 19) a) Frequency versus altitude, b) Modal amplitude versus longitudinal location along membrane.**

4.0 SIMULATING FLIGHT DYNAMICS OF FLEXIBLE VEHICLES

Many configurations such as high altitude long endurance vehicles, supersonic transports or blended wing body configurations show a potential for coupling of rigid body and flexible modes in what is called Body Freedom Flutter (BFF).[20-24] This phenomenon has been found in a number of aircraft, from the very light weight flying wing sailplanes to robust military aircraft.[21] The mechanism enabling BFF occurs as the aircraft velocity increases and the frequencies of the longitudinal short period mode and 1st wing bending mode approach one another. The short period frequency rises nearly linearly with airspeed while the wing bending frequency decreases with velocity as a result of increased aerodynamic damping. At the point where the short period frequency approaches the wing bending frequency, the physical coupling between pitch and wing bending produces a modal coupling which strongly affects the dynamics of the aircraft.[21] A range of issues is associated with BFF such as degradation of performance and loss of controllability. The result of unattenuated BFF is a catastrophic failure of the vehicle structure.

NASA Langley Research Center has recently collaborated with the Lockheed Martin Company in the computational aeroelastic analysis of the flutter characteristics of a conceptual design of a next generation supersonic transport, previously introduced in Figures 3-4. Static and dynamic aeroelastic analyses have been performed using both MSC.Nastran™ and the RANS code CFL3D. Results of the body freedom flutter simulation at Mach 0.8 using CFL3D is shown in Figure 8. Figure 9 shows a comparison of the flutter frequencies at Mach 0.8 and 1.2 computed with MSC.Nastran™ and CFL3D. At Mach numbers 0.8 and 1.2 static trim and body freedom flutter characteristics computed with MSC.Nastran™ and CFL3D compare well. The CFL3D code was used to compute flutter onset at Mach numbers 0.98 and 1.02 as well. Analyses at those Mach numbers show a relatively smooth variation in the flutter onset behavior through the sonic range.

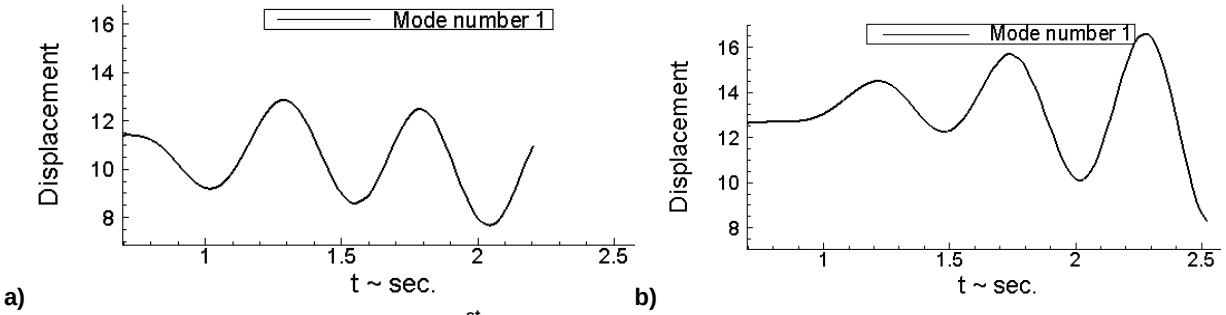

**Figure 8. Time history of 1st wing-body bending mode for supersonic transport
Mach 0.80. a) At flutter onset, b) Beyond flutter onset.**

Mach	RANS Flutter Freq (Hz)	NASTRAN Flutter Freq (Hz)
0.80	2.18	2.00
1.20	2.39	2.10

Figure 9. Flutter frequencies.

5.0 APPLICATIONS THAT SUPPORT BOTH AERONAUTICS AND SPACE EXPLORATION

Structured computational aeroelasticity codes have had a long standing role in aeroelastic analyses. Recently unstructured codes have begun to show promise as tools for computational aeroelastic analysis. Structured codes still find usefulness because of their efficiency. Unstructured codes, while much more computationally expensive, allow for fairly rapid grid generation for complex configurations. This is useful during the early design stage when a vehicle is undergoing rapid outer mold line changes.

Launch vehicles historically have been designed by empirical models tuned by steady and unsteady wind tunnel data. The effect of structural modes on steady state aerodynamics have been accounted for by use of 'bent' wind tunnel models. Even classical higher order analyses of flexible launch vehicles in the past have been performed in a quasi-coupled manner. That is, steady or unsteady computed aerodynamic loads are imposed on a structural model of the vehicle. References 25-27 discuss the potential of flow phenomena present in the ascent aerodynamics of hammerhead launch vehicles in producing instabilities that can compromise the structural integrity of the vehicle. The analysis technique in those references uses experimental data from wind tunnel tests coupled with analysis. Because the aerodynamic data is experimentally derived, this approach does not address the issue of scaling to full size. References 25 and 26 used a state-of-the-art CFD code to produce unsteady pressures at flight Reynolds number which then was applied to a structural model to simulate the buffeting response of the Titan IVB. Good agreement with transonic buffeting responses in flight were reported with this method.

Aeroelastic simulations using a full potential flow solver coupled with a vorticity transport model to account for viscous effects have calculated the aeroelastic behavior of a missile with a simple cylindrical finned geometry.[27-28] Other methods using slender body theory or linearized transonic flow have been applied to launch vehicles.[29-33] However very little fully coupled steady and unsteady computational aeroelastic analysis of launch vehicles using higher fidelity tools has been performed. Aeroelastic analyses of launch vehicles that incorporate full coupling of the structure and aerodynamics are of relatively recent use.

The NASA Ares I aeroelastic analysis team has been using the computational aeroelastic codes FUN3D and CFL3D to perform analysis of the Ares I crew launch vehicle (CLV). The configuration of the new Ares I CLV poses challenges to the design. The first stage is constructed from a five segment solid rocket booster (SRB) while the second stage houses liquid fuel and oxidizer tanks and thus has a larger diameter. The two stages are connected by an interstage frustum. This hammer head configuration has the potential to produce buffet induced by flow separation from the larger upper stage. Another challenge is the fact that the Ares I CLV is also the most flexible launch vehicle NASA has designed to date. These factors require careful aeroelastic analysis to ensure design integrity.

Analysis of ground wind loads is also required for a proper design of launch pad restraints. A launch vehicle on the pad in the presence of ground winds can exhibit vortex shedding. Vortex shedding can potentially cause large scale motion of a vehicle of the size and flexibility of the Ares CLV. This has motivated a ground wind loads test program using an aeroelastically-scaled CLV and an accompanying computational aeroelastic analysis. Computational aeroelastic analyses are being performed to assess the expected extent of motion of the vehicle. Figure 10 a) shows a launch vehicle similar to the Ares CLV mounted on a ground plane. This is the ground wind loads wind tunnel checkout model for which aeroelastic wind tunnel testing has been performed. The tunnel model was mounted in such a way to allow rotation of the model about a vertical axis via a floor mounted turntable. The angle θ represents the turntable angle. The model is cantilevered from the

base to simulate a launch vehicle clamped at the aft skirt but otherwise unrestrained. The unstructured code FUN3D has been used to perform aeroelastic analyses. Figure 10 b) shows a close up of the CFD surface mesh. A beam model of the vehicle has been used to simulate the wind tunnel model structural dynamics. Figure 11 shows the even numbered mode shapes of the wind tunnel scale model used in this analysis. The odd numbered modes that are not shown were orthogonal and had identical frequencies to their even numbered modal counterpart.

Dynamic analysis of this vehicle for a fully turbulent flow at a Mach number of 0.2, Reynolds number per first stage diameter of 2 million and turntable angle of 311^o reveals vortex shedding primarily from around the crew exploration vehicle. The region in which shedding occurs is shown in the contours of the maximum normalized pressure minus the minimum normalized pressure over a shedding cycle shown in Figure 12. The flexible vehicle solution shows these vortex flow characteristics potentially interacting with the first bending mode. Figure 13 shows the computed accelerations of the Launch Abort System (LAS) tower of this wind tunnel model to be in the range of plus or minus 1.5 g's.

A unique strength of computational simulation of a flexible launch vehicle is the ability to model fluid/thermal/structure interaction in the presence of roll control system (RCS) motors or the primary nozzle exhaust plume. Figures 14 shows the mesh about a generic launch vehicle. Figures 15-16 show the aeroelastic solution at a flight Mach number of 0.30 with and without an exhaust plume. The aft end of the vehicle nozzle serves as an exhaust inflow boundary having a total pressure ratio of 30 and a total temperature ratio of 10. These conditions result in an exhaust that enters the flow field at a Mach number of 5.6. The flow field is modelled as a single species perfect gas. By altering the pressure field over the aft region, the plume influences the flexible shape of the vehicle. This is clearly seen in the centerline deflection of the flexible vehicle shown in Figure 16.

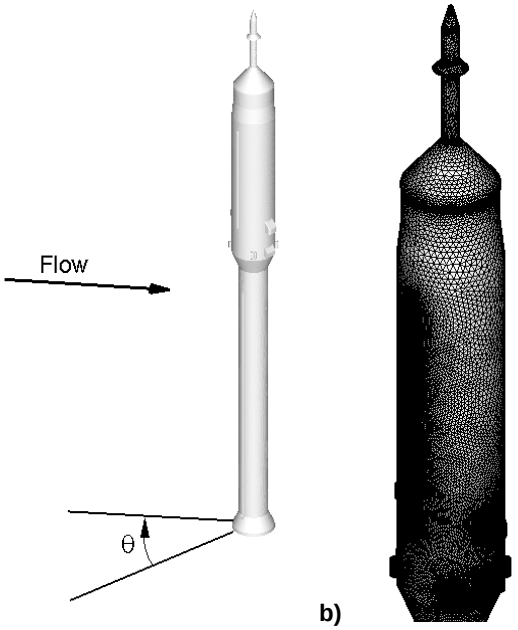

Figure 10. Ground wind loads model.
a) Model surface, turn table angle θ. b) CFD Surface mesh detail.

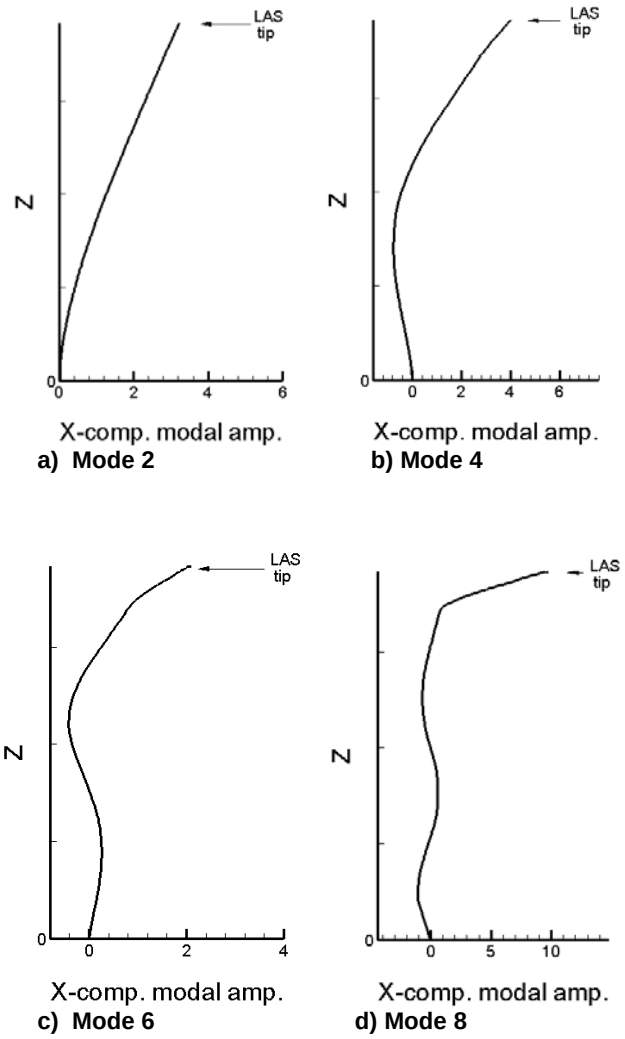

Figure 11. Mode shapes of the ground wind loads model.

Other concepts such as manned and unmanned atmospheric entry by the use of inflatable decelerator devices also require a design that accounts for fluid/structure interaction. This is an application that is difficult to fully test in a wind tunnel environment and is expensive to test in flight. For this reason towed and clamped inflatable ballute designs have been studied and recent aeroelastic analyses have been performed for both configurations.[15-17] Figure 17 shows an unstructured surface mesh for a towed ballute configuration. The oblique view shows the re-entry capsule in the foreground and the toroidal ballute in the background. The geometry shown in Figure 17 is based on the generic ballute configuration of reference 34. The unstructured CFD mesh and a MSC.Nastran[TM] finite element model are shown. Because of the high degree of flexibility of these devices, a computational aeroelastic analysis tool that can account not only for a nonlinear fluid and a nonlinear structural response but also thermal coupling of the fluid and structure is required.[18,34] A steady solution of this configuration using the unstructured code FUN3D is shown in Figure 18. A solution with the original grid and a solution using the grid adaptation in FUN3D are shown.

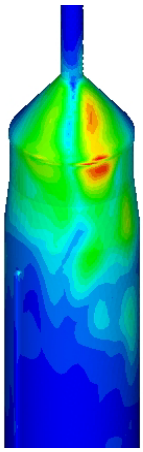

Figure 12. Ground wind loads model, Mach = 0.20, Re = 2 mill., θ = 311°. Contours of unsteady pressure $\Delta p/p_{inf} = (p_{max}-p_{min})/p_{inf}$.

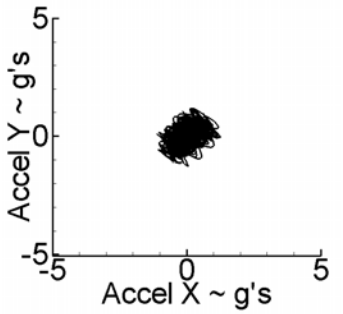

Figure 13. Acceleration at tip of LAS tower, , Mach = 0.20, Re = 2 mill., θ = 311°.

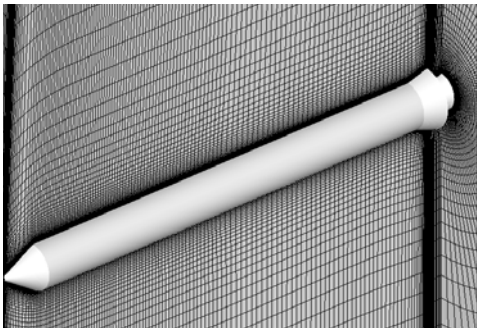

Figure 14. Generic launch vehicle CFD grid.

a) 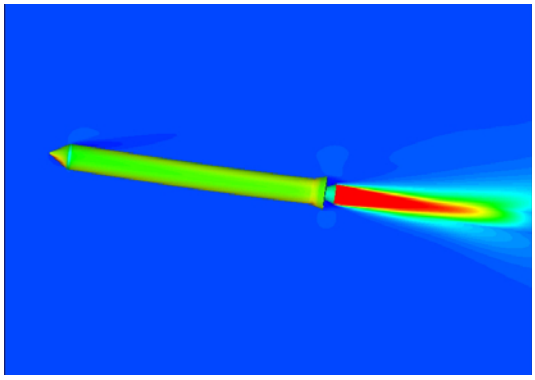 b) 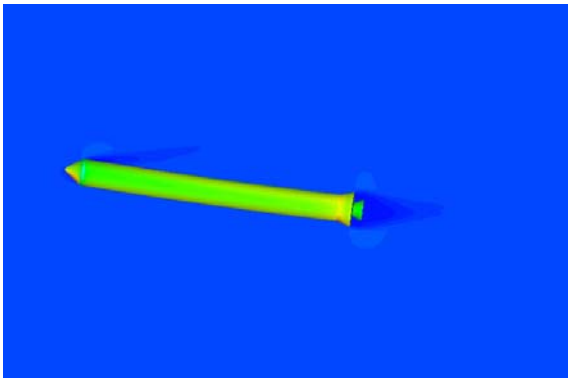

Figure 15. Generic launch vehicle aeroelastic solution, Mach 0.3, α = 20 degrees. Surface contours are of Cp while flow field contours are of Mach number. a) with plume, b) without plume.

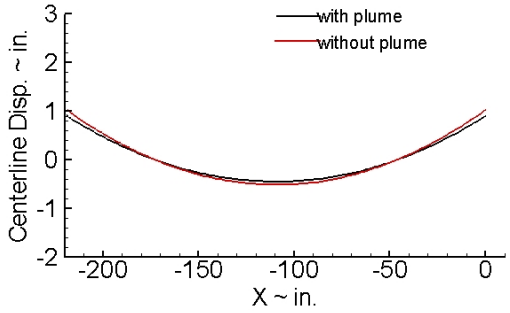

Figure 16. Generic launch vehicle centerline displacement, Mach 0.3, α = 20 degrees.

a) 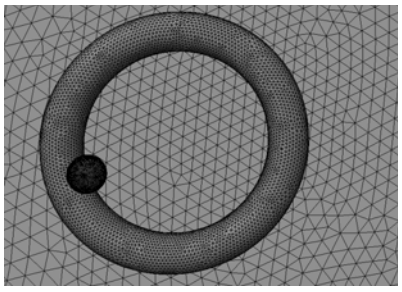 b) 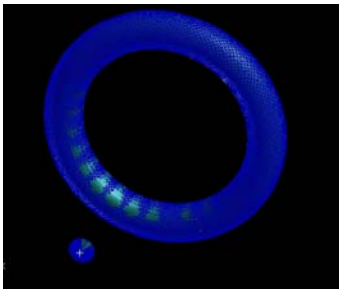

Figure 17. Atmospheric reentry vehicle and towed inflated ballute.
a) Unstructured CFD mesh, b) MSC.Nastran™ finite element model.

a) 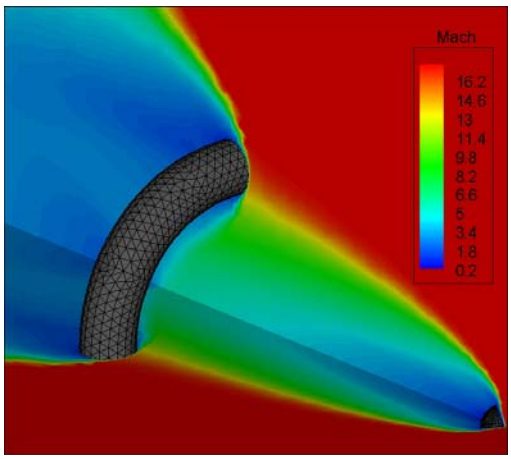

b) 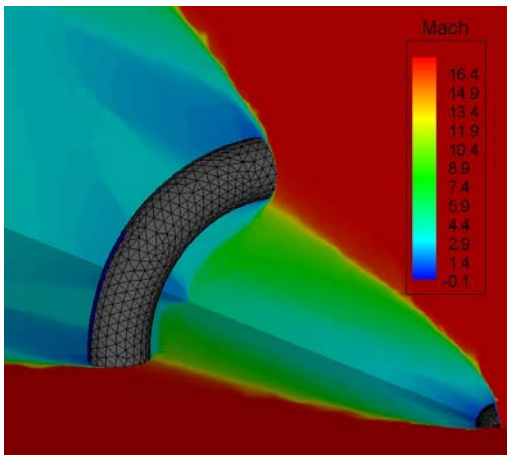

Figure 18. Atmospheric reentry vehicle and towed inflated ballute, Mach contours. a) Using original grid, b) Using solution adapted grid.

5.0 CONCLUDING REMARKS

Computing resources have progressed and computational aeroelastic analysis tools have achieved a level of fidelity that has allowed the use of these tools in a growing number of applications. Many of these applications are for conditions that are not easily tested in a wind tunnel. This provides a unique challenge and opportunity to perform analyses and acquire data for vehicle design not possible for past flight and launch vehicles. There are many problems for which computational aeroelastic tools are increasingly being applied. The present paper has discussed a range of applications for which higher fidelity computational aeroelastic tools have been used at the NASA Langley Research Center.

6.0 REFERENCES

1. Batina, J. T., Seidel, D. A., Bland, R. R., Bennet, R. M., "Unsteady transonic flow calculations for realistic aircraft configurations," *Journal of Aircraft,* Vol. 26, No. 1, pp. 21-28, 1989.
2. Edwards, J. W., "Transonic shock oscillations calculated with a new interactive boundary layer coupling method." 31st Aerospace Sciences Meeting and Exhibit. AIAA paper 1993-0777.
3. Edwards, J. W., Calculated Viscous and Scale Effects on Transonic Aeroelasticity. Paper No. 1 in AGARDD-R-822, "Numerical Unsteady Aerodynamics and Aeroelastic Simulation," March 1998. Presented at the 85th Meeting of the AGARD Structures and Materials Panel, Aalborg, Denmark, October 14-15, 1997.
4. Bartels, R. E., Rumsey, C. L., Biedron, R. T., "CFL3D Version 6.4 – General usage and Aeroelastic Analysis," NASA/TM-2006-214301, April 2006.
5. Anderson, W. K., and Bonhaus, D. L., "An Implicit Upwind Algorithm for Computing Turbulent Flows on Unstructured Grids," *Computers and Fluids*, Vol. 23, No. 1. pp. 1-21, 1994.
6. Biedron, R. T., Vatsa, V. N., and Atkins, H. L., "Simulation of Unsteady Flows Using an Unstructured Navier-Stokes Solver on Moving and Stationary Grids," AIAA paper 2005-5093.
7. Conner, M. D., Tang, D. M., Dowell, E. H., Virgin, L. N., "Nonlinear behavior of a typical airfoil section with control surface freeplay: A numerical and experimental study," *Journal of Fluids and Structures*. Vol. 11, No. 1, No. , pp. 89-109, 1997.
8. Tang, D. M., Dowell, E. H., Virgin, L. N., "Limit cycle behavior of an airfoil with a control surface," *Journal of Fluids and Structures* , Vol. 12, No. 7, pp. 839-858, 1998.

9. Kuruvila G., Bartels R. E., Hong, M. S., Bhatia, K. G., "Nonlinear Aeroelastic Analysis Using a Time-Accurate Navier-Stokes Equations Solver," CEAS/AIAA/ICASE/NASA Internationial Forum on Aeroelasticity and Structural Dynamics, June 2007.
10. Bibb, K. L., Gnoffo, P. A., Park, M. A., Jones, W. T., "Parallel, Gradient-Based Anisotropic Mesh Adaptation for Re-entry Vehicle Configurations," 9th AIAA/ASME Joint Thermophysics and Heat Transfer Conference, June 5-8 2006, San Francisco, CA.
11. Lee-Rausch, E. M., Park, M. A., Jones, W. T., Hammond, D. P., and Nielsen, E. J., "Application of a Parallel Adjoint Based Error Estimation and Anisotropic Grid Adaptation for Three-Dimensional Aerospace Configurations," AIAA paper 2005-4842.
12. Jones, W. T., Nielsen, E. J., and Park, M. A., "Validation of 3D Adjoint Based Error Estimation and Mesh Adaptation for Sonic Boom Prediction," AIAA paper 2006-1150.
13. Jones, W. T., "GridEx – An Integrated Grid Generation Package for CFD," AIAA Paper 2003-4129.
14. Haimes, R., "CAPRI: Computational Analysis PRograming Interface," Proceedings of the 6th International Conference on Numerical Grid Generation in Computational Field Simulations, July 1998.
15. Rohrschneider, R. R., Braun, R. D., "Aeroelastic Design Considerations of a Clamped Ballute for Titan Aerocapture," 48th AIAA/ASME/ASCE/AHS/ASC Structures, Structural Dynamics, and Materials Conference, 23-26 April 2007,Honolulu, Hawaii.
16. Lee, J., Rohrschneider, R. R., Ruffin, S. M., Braun, R. D., "Fluid-Structure Analysis of a Clamped Ballute in Titan's atmosphere," 18th Computational Fluid Dynamics Conference, 25-28 June 2007, Miami, FL.
17. Rohrschneider, R. R., Braun, R. D., "Survey of Ballute Technology for Aerocapture," *Journal of Spacecraft and Rockets*, Vol. 44, No. 1, January-February 2007.
18. Bartels, R. E., Moses, R. W., Scott, R. C., Templeton, J. D., Cheatwood, F. M., Gnoffo, P. A, Buck, G. M., "A Proposed Role of Aeroelasticity in NASA's New Exploration Vision", CEAS/AIAA/ ICASE/NASA Internationial Forum on Aeroelasticity and Structural Dynamics, June 2005, Munich.
19. Scott, R. C., Bartels, R. E., Kandil, O. A., "An Aeroelastic Analysis of a Thin Flexible Membrane," 48th AIAA/ASME/ASCE/AHS/ASC Structures, Structural Dynamics, and Materials Conference, 23-26 April 2007, AIAA paper 2007-2316.
20. Banerjee, J. R., "Flutter Characteristics of High Aspect Ratio Tailless Aircraft," *Journal of Aircraft,* Vol. 21, No. 9, 1984, pp. 733-736.
21. Love, M. H., Zink, P. S., Wieselmann, P. A., Youngren, H., "Body Freedom Flutter of High Aspect Ratio Flying Wings," 16th AIAA/ASME/ASCE/AHS/ASC Structures, Structural Dynamics & Materials Conference, 18-21 April 2005, Austin, TX, AIAA paper 2005-1947.
22. Patil, M. J., Hodges, D. H., "Flight Dynamics of Highly Flexible Flying Wings," *Journal of Aircraft*, Vol. 43, No. 6, 2006, pp. 1790-1798.
23. Su, W., Cesnik, C. E. S., "Dynamic Response of Highly Flexible Flying Wings," 47th AIAA/ASME/ASCE/AHS/ASC Structures, Structural Dynamics, and Materials Conference, 1-4 May 2006, Newport, RI, AIAA paper 2006-1636.
24. Snyder, M. P., Sanders, B., Eastep, F. E., Frank, G. J., "Vibration and Flutter Characteristics of a Folding Wing," 46th AIAA/ASME/ASCE/AHS/ASC Structures, Structural Dynamics & Materials Conference, 19-21 April 2005, Austin, TX, AIAA paper 2005-1994.
25. Ericsson, L. E., "Hammerhead Wake Effects on Elastic Vehicle Dynamics," *Journal of Spacecraft and Rockets*, Vol. 34, No. 2, March-April 1997.
26. Ericsson, L. E., "Unsteady Flow Separation Can Endanger the Structural Integrity of Aerospace Launch Vehicles," *Journal of Spacecraft and Rockets*, Vol. 38, No. 2, March-April 2001.
27. Reisenthel, P., Lesieutre, D. J., Nixon, D., "Prediction of Aeroelastic Effects for

Sea-Skimming Missiles with Flow Separation, " AIAA paper 1991-1052-CP.
28. Lesieutre, D. J., Reisenthel, P. H., Dillenius, M. F., Viazzo, D., Fisher, S., Bhat, S., McIntosh, S. C., "Unsteady Simulation of Flexible Missiles Flying Low Over the Sea," AIAA paper 1994-0720.
29. Reisenthel, P. H., Nixon, D., " Prediction of Unsteady Separated Transonic flow Around Missile Configurations, " AIAA paper 1991-0601.
30. Chen, P. C., Sulaeman, E., Liu, D. D., Auman, L. M., "Body-Flexure Control with Smart Actuation for Hypervelocity Missiles," AIAA paper 2003-1965.
31. Chen, P. C., Liu, D. D., "Unsteady Wing-Body Aerodynamics for Aeroelastic Applications at Mach One," *AIAA Journal*, Vol. 44, No. 8, August 2006.
32. Liu, D., D., "Quasi-Slender Body Theory for Unsteady Linearized Transonic Flow Past Pointed Bodies of Revolution," Lockheed Missiles and Space Company LMSC/HREC A791435, Huntsville, AL, April 1968.
33. Chen, P. C., Gao, X. W., Tang, L., "An Overset Field-Panel Method for Unsteady Transonic Aerodynamic Influence Coefficient Matrix Generation," AIAA paper 2004-1512.
34. Gnoffo, P. A., Anderson, B. P. "Computational Analysis of Towed Ballute Interactions," AIAA paper 2002-2997.